# OPPOSING MICROTUBULE MOTORS CONTROL MOTILITY, MORPHOLOGY, AND CARGO SEGREGATION DURING ER-TO-GOLGI TRANSPORT.

ANNA K. BROWN, SYLVIE D. HUNT, AND DAVID J. STEPHENS*

CELL BIOLOGY LABORATORIES, SCHOOL OF BIOCHEMISTRY, MEDICAL SCIENCES BUILDING, UNIVERSITY OF BRISTOL, BS8 1TD TEL: 00 44 117 331 2173

*CORRESPONDING AUTHOR. EMAIL: DAVID.STEPHENS@BRISTOL.AC.UK

† NÉE ANNA K. TOWNLEY

## 1 SUMMARY

2 We recently demonstrated that dynein and kinesin motors drive multiple aspects of endosomal function in mammalian
3 cells. These functions include driving motility, maintaining morphology (notably through providing longitudinal tension
4 to support vesicle fission), and driving cargo sorting. Microtubule motors drive bidirectional motility during traffic
5 between the endoplasmic reticulum (ER) and Golgi. Here, we have examined the role of microtubule motors in
6 transport carrier motility, morphology, and domain organization during ER-to-Golgi transport. We show that consistent
7 with our findings for endosomal dynamics, microtubule motor function during ER-to-Golgi transport of secretory cargo
8 is required for motility, morphology of, and cargo sorting within vesicular tubular carriers *en route* to the Golgi. Our
9 data are consistent with previous findings that defined roles for dynein-1 and kinesin-1 (KIF5B) and kinesin-2 in this
10 trafficking step. Our high resolution tracking data identify some intriguing aspects. Depletion of kinesin-1 reduces the
11 number of motile structures seen which is in line with other findings relating to the role of kinesin-1 in ER export.
12 However, those transport carriers that were produced had a much greater run length suggesting that this motor can act
13 as a brake on anterograde motility. Kinesin-2 depletion did not significantly reduce the number of motile transport
14 carriers but did cause a similar increase in run length. These data suggest that kinesins act as negative regulators of ER-
15 to-Golgi transport. Depletion of dynein not only reduced the number of motile carriers formed but also caused
16 tubulation of carriers similar to that seen for SNX-coated early endosomes. Our data indicated that the previously
17 observed anterograde-retrograde polarity of transport carriers in transit to the Golgi from the ER is maintained by
18 microtubule motor function.

19

## 20 INTRODUCTION

21 Endoplasmic reticulum (ER)-to-Golgi transport is required for the delivery of newly synthesized secretory cargo to the
22 Golgi apparatus. Following the concentration of cargo and budding of carriers at the ER, cargo accumulates in the ER-
23 Golgi intermediate compartment (ERGIC) from which it is then transported to the Golgi. Transport of cargo in small
24 vesicular tubular transport carriers between the ER and Golgi along microtubules ensures vectorial delivery of cargo in
25 an efficient manner (Ho et al., 1989; Lippincott-Schwartz et al., 1990; Thyberg and Moskalewski, 1985). The link to
26 microtubules is established at the point of ER export through direct interaction of the Sec23 subunit of the COPII coat
27 complex with the p150[Glued] subunit of dynactin (Watson et al., 2005). It is not known how the ERGIC is itself linked to
28 microtubules but considerable data have shown that cytoplasmic dynein-1 is required for the movement of cargo in
29 VTCs to the Golgi (Burkhardt et al., 1997; Palmer et al., 2009; Presley et al., 1997). Other work has identified roles for
30 kinesin-1 in ER export and in retrograde transport from the Golgi back to the ER (Lippincott-Schwartz et al., 1995).

31    Kinesin-2 also acts in retrograde traffic from the Golgi (Stauber et al., 2006). Recently, we used RNAi-mediated
32    depletion of individual microtubule motor subunits to define their function in the endosomal system (Hunt et al., 2013).
33    Using GFP-tagged sorting nexins (SNXs) and total internal reflection fluorescence (TIRF) microscopy to maximize signal-
34    to-noise ratios, we found that specific combinations of microtubule motors were coupled to individual sorting SNX-
35    coated membrane domains.

36    We showed that these specific combinations of motors direct not only the motility of these endosomal domains but
37    also dictate their morphology and the segregation of cargo within them. Our data are consistent with models in which
38    longitudinal tension, generated by the motor acting on a membrane (Roux et al., 2002), aids in the scission event that
39    generates small transport carrier from larger compartments (reviewed in (Stephens, 2012)). This longitudinal tension
40    could form part of a geometric sorting process driving cargo segregation into distinct functional domains (Mayor et al.,
41    1993). Since ER-to-Golgi transport, like early endosomal motility, is known to use cytoplasmic dynein-1 in combination
42    with kinesin-1 and kinesin-2, we chose to apply the same technique to the transport of secretory cargo from the ER to
43    the Golgi. We chose tsO45-G-GFP for this process as this viral glycoprotein is widely used model cargo and provides a
44    means to initiate cargo trafficking through temperature-controlled. At 39.5$^{o}$C tsO45-G-GFP is retained in the ER; at 32$^{o}$C
45    it folds and rapidly exits the ER using the same machinery as other endogenous cargo. While a non-homologous system,
46    the benefits of being able to image transport in a controlled way outweigh the limitations. Furthermore, the increase in
47    signal to noise ratio using of TIRF microscopy allowed us to use this probe at a relatively low expression. We use TIRF
48    microscopy here not to provide a selective illumination of events very close to the plasma membrane but instead with
49    an increased penetration depth to facilitate this increase in signal-to-noise.

50    Previous work has shown that tsO45-G-GFP is trafficked in vesicular tubular clusters to which the COPI coat complex is
51    recruited. COPI directs retrograde sorting of membrane proteins from the Golgi to the ER and a widely accepted model
52    is that this retrograde recycling is initiated at the ERGIC and continues during transit of cargo to the Golgi. An
53    interesting feature of this process is that COPI localizes to the retrograde domain of these carriers while secretory cargo
54    such as tsO45-G-GFP accumulates in the Golgi-facing or anterograde domain (Shima et al., 1999). This domain-based
55    segregation of cargo is reminiscent of that seen in the endosomal pathway.

56    Here we have taken this same approach of motor subunit depletion using RNAi coupled with TIRF imaging to examine
57    the role of microtubule motors in the dynamics of transport carriers moving from the ER to the Golgi.

58

## RESULTS

60    We used TIRF imaging of cells expressing the temperature sensitive form of the vesicular stomatitis virus glycoprotein
61    (ts045-G) tagged with GFP. This enables controlled release of this model secretory cargo from the ER such that we can
62    unequivocally identify structures during the early stages of transit to the Golgi (<12 minutes after release of the
63    temperature block). From analysis of many experiments, we determined that the number of detectable ts045-G-GFP-
64    positive structures was decreased following either dynein-1 or kinesin-1 depletion (but not that of other motors) the
65    proportion of motile structures was not changed. This decrease in formation of VTCs is consistent with our previous
66    work (Gupta et al., 2008). Motor protein depletion was achieved using siRNA transfection and validated by
67    immunoblotting periodically through the project (see also (Hunt et al., 2013; Palmer et al., 2009)).

68    Figure 1 shows maximum intensity projections of the transport of tsO45-G-GFP starting 12 minutes after the shift to
69    32$^{o}$C. These are derived from the movie sequences shown in the associated movie files. Two versions of each movie are
70    included, one playing back at real time, and another playing back at 3x speed. In control cells (Fig. 1A-C, Movie 1A and
71    Movie 1B) many tracks are evident that translocate towards the Golgi. We then performed the same assay in cells that
72    had previously been depleted of individual motor subunits prior to expression of tsO45-G-GFP. Suppression of dynein
73    heavy chain 1 (DHC1) resulted in fewer visible carriers translocating to the Golgi (Fig. 1D, Movie 2A and Movie 2B). An
74    immediate feature of the maximum intensity projections is that the length of individual tracks is much shorter (Fig. 1E, F
75    and see below). Many small punctate carriers were still visible which we attribute to the incomplete loss of DHC1
76    expression in these experiments. Our interpretation is therefore based on changing the balance of cellular motor

77  subunits and not the presence or absence of any individual component. In our own work, we have previously defined a
78  role of the light intermediate chain 1 (LIC1) of cytoplasmic dynein 1 in Golgi organization and ER-to-Golgi transport
79  (Palmer et al., 2009).  Here we found that depletion of LIC1 led to a similar but less dramatic phenotype to depletion of
80  DHC1 (Fig. 1G, Movie 5A and Movie 5B). Notably an increase in the number of static structures and those only moving a
81  very short distance was evident (Fig. 1H, enlarged in I). KIF5B had previously been implicated in the export of cargo
82  from the ER (Gupta et al., 2008) and kinesin-2 has also been implicated in Golgi-to-ER retrograde trafficking (Stauber et
83  al., 2006). In many other systems motors of opposing polarity are essential for movement in either direction (Ally et al.,
84  2009). Here we found that in contrast to depletion of dynein subunits where motility was reduced, kinesin-1 depletion
85  led to increased movement of tsO45-G-GFP along continuous tracks that were substantially longer than seen in controls
86  (Figure 1J-L, Movie 3A and Movie 3B). A similar result, although less noticeable, was seen following depletion of kinesin-
87  2 (achieved by targeting the KAP3 accessory subunit of this motor, Figure 1M-O, Movie 4A and Movie 4B).

88  Quantification of these data is presented in Figure 2. Depletion of either DHC1 or KIF5B significantly reduced the
89  number of motile transport carriers (defined as those moving >5 µm) that we observed (Fig. 2A). This likely reflects the
90  known function of these motors in ER export (Gupta et al., 2008) and transport carrier motility (Presley et al., 1997).
91  This contrasts with our findings in relation to endosomal motility where opposing motors are both required to drive
92  motility (Hunt et al., 2013) and peroxisome motility (Ally et al., 2009). We then measured the movement of objects
93  based on track length from maximum intensity projections from time sequences of 50 seconds duration. In all cases, we
94  found that the speed of individual moving structures was the same regardless of gene depletion using RNAi, ranging
95  from 0.2-3.1 $\mu m.sec^{-1}$. Fig. 2B shows the spread of track lengths for individual structures measured from maximum
96  intensity projections of time sequences. In control cells a range of track lengths between 0 and 160 µm was measured.
97  Depletion of DHC1 led to a significant reduction in track length; the mean track length was also decreased on
98  suppression of LIC1 but this difference was not statistically significant. Of note, the longest tracks in this case are those
99  that are lost. We conclude from these plots, and the image data in Fig. 1, that LIC1 suppression was less effective at
100 inhibiting motility of these structures perhaps due to partial redundancy with LIC2 or due to incomplete suppression. In
101 this study, we have not analyzed cells following LIC2 suppression only as our previous work strongly implicated LIC1 in
102 Golgi-related functions of dynein (Palmer et al., 2009). Somewhat surprisingly, depletion of either kinesin-1 or kinesin-2
103 resulted in a statistically detectable increase in track length (Fig. 2, green asterisks indicate a statistically detectable
104 increase in track length). The statistical tests are consistent with the visual impression of the data shown in Fig. 1 that
105 kinesin-2 depletion is less effective than that of KIF5B. These data imply that kinesins act against dynein in this system
106 to attenuate motility of ER-to-Golgi transport carriers.

107 From our work on the endosomal system, we determined that microtubule motors were required to maintain the
108 morphology of endosomes (Hunt et al., 2013). Depletion of individual motor subunits led to tubulation of SNX-labelled
109 endosomal compartments. We have previously documented a similar effect on early ER-to-Golgi transport carriers
110 following KIF5B depletion (Gupta et al., 2008). Here, in our TIRF time-lapse sequences tracking the movement of tsO45-
111 G-GFP from the ER to the Golgi we observed a similar, although less dramatic, increase in tubulation following DHC1
112 suppression (Fig. 3, multiple examples are shown that are taken from the time sequence in Fig 1D and movie 2).
113 Tubules were occasionally seen in control movies (1-2 per cell in the 50 second time sequences acquired) but were
114 more obvious in DHC1-depleted cells (3-10 per cell). Tubules were typically short (< 5 µm), highly motile, and were
115 occasionally branched (Fig. 3A). Other work has shown that tubulation of ER-to-Golgi carriers is linked to the level of
116 cargo expression (Simpson et al., 2006). Analysis of fluorescence intensity in the data sets described here indicates that
117 the increased tubulation seen here is due to DHC1 suppression and not an increase in tsO45-G-GFP expression in these
118 selected cases (not shown). These data are consistent with work showing that tubular transport intermediates are
119 dependent on an intact microtubule network (Simpson et al., 2006), and that describing the formation of highly
120 dynamic ERGIC tubules following motor depletion (Tomas et al., 2010).

121 Analysis of the role of motor subunits in the endosomal system also led us to define a role in segregation of endocytic
122 cargo into distinct functional domains (Hunt et al., 2013). Previous work has shown that ts045-G-GFP localizes to an
123 anterograde (i.e. Golgi facing) domain of the transport intermediate during its transit to the Golgi (Shima et al., 1999).
124 The COPI complex provides a marker of the retrograde domain. We used these markers in fixed cells, 12 minutes after
125 temperature shift to $32^{o}C$ to ask whether dynein and kinesin motors are required to maintain this domain organization.

126   Objects were measured by visual inspection with the Golgi defined as the centre of the brightest cluster of objects
127   (denoted with the letter "G" in Fig. 4A). Here it is important to note that depletion of DHC1 causes significant disruption
128   to Golgi structure, resulting in the presence of multiple small Golgi elements throughout the cytoplasm. This
129   complicates analysis here likely leading to an under estimation of the degree of COPI-association with bona fide ER-to-
130   Golgi transport carriers and likely an inaccurate assessment of their polarity. Regardless, we include these data for
131   completeness. Fig. 4A shows and example of these image data from control cells (GL2 siRNA transfected). Green arrows
132   indicate the position of tsO45-G-GFP and red arrows the position of COPI. Insets 1, 2, and 4, show a polarization of the
133   structure with the green domain closer to the Golgi (indicated by the letter "G"). Inset 3 shows an object of the
134   opposite polarization with the COPI-positive domain facing the Golgi. We measured two parameters from these data:
135   the number of tsO45-G-GFP puncta that were positive for COPI, and the polarization of these structures with regard to
136   the Golgi. Fig. 4B shows the proportion of tsO45-G-GFP structures that were positive for COPI. Gray bars indicate the
137   mean. Depletion of LIC1, KIF5B, or KAP3 did not affect the association of COPI with these structures. This is consistent
138   with the known mechanisms of recruitment of COPI to membranes and is suggests that these motor subunits are not
139   required for the recruitment of COPI.  While a statistically significant decrease in COPI association is seen following
140   DHC1 depletion, we attribute this to the fragmentation of the Golgi apparatus in these cells and the fact that even at 12
141   minutes after temperature shift, there is a substantial proportion of tsO45-G-GFP in the early Golgi. In contrast, when
142   we measured the orientation of tsO45-G-GFP and COPI positive structures, we found that depletion of any of the four
143   motor subunits resulted in a decrease in the proportion of correctly polarised objects (Fig. 4C). In particular, depletion
144   of LIC1 or of KAP3 resulted in a statistically detectable decrease in this measure (Fig 4C, red asterisks). The microtubule
145   network was not perturbed significantly in these cells (see (Gupta et al., 2008; Hunt et al., 2013; Palmer et al., 2009))
146   and thus, we conclude that these motors are required to either generate or maintain this domain organization.

147   We then sought to define whether there was any obvious defect in ER-to-Golgi cargo trafficking. For this we chose to
148   analyse the distribution of KDEL-bearing proteins which under normal circumstances are retained in the ER by active
149   retention and retrieval mechanisms. We reasoned that a possible defect in COPI-dependent retrieval following motor
150   subunit depletion might manifest itself as an increase in anterograde transport of KDEL-bearing cargoes.
151   Immunoblotting (Fig. 4D) and immunofluorescence (Fig. 4D, showing images of control and KIF5B siRNA transfected
152   cells) of KDEL-bearing proteins revealed no differences in steady-state localization in control versus motor subunit
153   depleted cells.

154

## DISCUSSION

156   The importance of the microtubule motor system to mammalian cell organization and function is unquestionable. Our
157   knowledge of the mechanochemistry of these enzymes, as well as the ways in which they are targeted to specific
158   intracellular cargoes is increasing rapidly. In this study, we have extended our work examining the role of individual
159   motor subunits in the endocytic pathway to the biosynthetic secretory pathway. This has highlighted several common
160   features and some notable differences. In general terms we can conclude that in both the endocytic and biosynthetic
161   systems, microtubule motors act not only in the motility of these small vesicular and tubular carriers but also in
162   maintaining their structure, and in maintaining (and possibly generating) the functionally distinct domains within these
163   complex structures.

164   Our data also highlight cross-talk between motors of opposing polarity, dynein and the kinesins, in ER-to-Golgi
165   transport. Suppression of KIF5B expression results in longer linear tracks of tsO45-G-GFP suggesting that it normally acts
166   as a negative regulator of run length, probably through opposing the minus-end directed force of dynein. The normal
167   balance of opposing motors that frequently engage in a tug-of-war (Derr et al., 2012) is likely imbalanced by our KIF5B
168   gene depletion experiments such that we bias movement towards the minus end. That we observe this effect more
169   robustly with KIF5B depletion than KAP3 depletion suggests that dynein-1 opposing kinesin-1 is the most common tug-
170   of-war in this ER-to-Golgi trafficking step. While we can clearly identify these changes in transport carrier motility
171   following motor subunit depletion we have been unable to define any functional consequence of this. KIF5B depletion
172   does slow the overall rate of cargo trafficking (Gupta et al., 2008) but only at later stages release of tsO45-G-GFP from
173   the ER. The Golgi remains *cis-trans* polarized in the same way that it is in control cells, we do not observe any gross

4

174 defect in retrograde trafficking of KDEL tagged cargo in KIF5B depleted cells (which used uses the COPI system in
175 concert with the KDEL receptor (Lewis and Pelham, 1990; Munro and Pelham, 1987)).

176 It is possible, even probable that defects in these motor-dependent trafficking events on manifest themselves as gross
177 phenotypic consequences in cell types that have a significant dependence on long range microtubule-based transport.
178 An obvious example would be motor neurons and this is of course consistent with the fact that many mutations in
179 dynein subunits, kinesins, and their accessory molecules result in severe neurological defects (recently reviewed in
180 (Franker and Hoogenraad, 2013)). We have not undertaken any experiments to address this at present.

181 The identity of the molecular linkers between these motors and the membranes that they carry are still not well
182 defined. Recent work has identified the Golgi matrix protein golgin-160 as a key determinant of dynein localization to
183 the Golgi (Yadav et al., 2012). Whether golgin-160 is the specific, or indeed the only, dynein anchor in ER-to-Golgi
184 transport of anterograde cargo remains unclear. This is an important question as the molecular basis for trafficking
185 through the early secretory pathway is still poorly understood. It is know that COPII mediates the export of cargo from
186 the ER. COPII-derived vesicles then either fuse together homotypically or fuse with a pre-existing ER-Golgi intermediate
187 compartment (ERGIC). The subsequent transport step remains something of a mystery. Is there a budding event from
188 the ERGIC or are large parts of this organelle separated from the underlying structure prior to transport to the Golgi?
189 This latter option could clearly involve the application of force by motor proteins, notably dynein, in an analogous way
190 to the role of kinesin at the *trans*-Golgi network (Polishchuk et al., 2003). Analysis of these options is complicated by the
191 fact that perturbation of the ERGIC often results in an inhibition of COPII-derived budding. An example is the use of
192 brefeldin A and other GBF1 inhibitors that while acting on recruitment of COPI through inhibiting Arf activation result in
193 accumulation of secretory cargo, not in the ERGIC, but in the ER (Lippincott-Schwartz et al., 1989). Clearly the
194 identification of factors that control motor recruitment and activation on ERGIC and transport carrier membranes will
195 help solve these questions.

196

## MATERIALS AND METHODS

198 All reagents were purchased from Sigma-Aldrich (Poole, UK) unless otherwise stated.

### GROWTH OF CULTURE CELLS
200 Human telomerase immortalized retinal pigment epithelial cells (hTERT-RPE1) were maintained in DMEM-F12
201 supplemented with 10% FCS (Life Technologies, Paisley, UK) containing supplemented 1% L-glutamine and 1% essential
202 amino-acids. At 24 hours prior to the start of the experiments, cells were seeded onto 35 mm glass bottom dishes
203 (MatTek, Ashland, MA).

### SOURCE OF ANTIBODIES AND OTHER REAGENTS
205 Monoclonal rat anti-human tubulin (ab6160) and polyclonal rabbit anti-KIF5B (ab5629) were from Abcam (Cambridge);
206 polyclonal rabbit anti-human kinesin-2 (kindly provided by Isabelle Vernos, Barcelona, Spain); polyclonal rabbit anti-
207 human lamin A/C (#2032) was from Cell Signaling Technology (Danvers, MA). Secondary antibodies were from Jackson
208 ImmunoResearch Laboratories (West Grove, PA). Anti-KDEL antibody (clone 10C2) was from Abcam.

### SMALL INTERFERING RNA TRANSFECTION
210 Cells were siRNA-transfected by calcium phosphate method at 3% $CO_2$ (Chen and Okayama, 1988). The medium was
211 changed 20 hours after transfection and cells were washed with PBS and were incubated for 72 hours at 37°C at 5% $CO_2$
212 with fresh supplemented media. SiRNA duplexes were designed using online algorithms of, and subsequently
213 synthesized by, MWG-Eurofins. BLAST search was performed for these duplexes against the non-redundant database to
214 determine their specificity. Lamin A/C or luciferase GL2 were depleted as targeted controls. Sequences used were as
215 follow: DHC1-a ACA UCA ACA UAG ACA UUC ATT; DHC1-b CCA AGC AGA UAA GGC AAU ATT; KIF5B-a UGA AUU GCU
216 UAG UGA UGA ATT; KIF5B-b UCA AGU CAU UGA CUG AAU ATT; KAP3-a CUU GAC CAU UCC AGA CUU ATT; KAP3.b GCU
217 CUG UGU AUG AAU AUU ATT; DLIC1-a AGA UGA CAG UGU AGU UGU ATT; DLIC1-b GAA CAU GAC UAC AGA GAU GTT;
218 Lamin A/C CUG GAC UUC AAG AAG AAC ATT; GL2 CGU ACG CGG AAU ACU UCG AUU TT.

219  TRANSIENT PLASMID EXPRESSION

220  Transient expression of tsO45-G-GFP was done using Lipofectamine™ 2000 as per manufacturer's instructions.

221  IMMUNOLABELLING

222  Medium was removed and cells were subsequently washed with PBS. Cells were then fixed using cold methanol for 4
223  minutes at -20°C. After two washes in PBS, cells were blocked using a 3% bovine serum albumin (BSA) in PBS for 30
224  minutes at room temperature. Cells were incubated with the primary antibodies (anti-beta'-COP rabbit polyclonal
225  "BSTR") in 3% BSA for 1 hour at room temperature. Three washes with PBS of 5 minutes each at room temperature
226  were done before incubating the secondary antibody. The latter was diluted at 1:400 in PBS and incubated 1 hour at
227  room temperature. Finally, after three washes in PBS (5 minutes each at room temperature) and an optional nuclear
228  staining with DAPI (4,6-Diamidino-2-phenylindole, Molecular Probes, diluted at 1:5000 in distilled water) for 3 minutes
229  at room temperature, cells were gently rinsed twice in PBS.

230  IMMUNOBLOTTING

231  For immunoblots to validate siRNA efficacy (not shown but for examples see (Gupta et al., 2008; Hunt et al., 2013;
232  Palmer et al., 2009)), cells were lysed and samples were separated by SDS-PAGE followed by transfer to nitrocellulose
233  membranes; primary antibodies were detected using HRP-conjugated secondary antibodies (Jackson ImmunoResearch,
234  West Grove, PA) and enhanced chemiluminescence (ECL, GE Healthcare, Cardiff, United Kingdom). For analysis of KDEL
235  protein secretion (Fig. 4) blots were developed using fluorophore conjugated secondary antibodies and an Odyssey Sa
236  imaging system (LI-COR Biosciences, Cambridge, UK).

237  TIRF IMAGING

238  Cells were kept at 37°C and at 5% CO2. Media was discarded and replaced with pre-warmed imaging medium (Life
239  Technologies) just prior imaging. The TIRF system used was a Leica AM-TIRF MC (multi colour) associated with a Leica
240  DMI 6000 inverted microscope. Images were acquired with an oil immersion TIRF objective with 100x 1.46 numerical
241  aperture and were acquired at the rate 12.04 frames per second (i.e. the interval between images was 83 ms) using a
242  Hamamatsu C9100-13 EMCCD camera. Each image was 512 by 512 pixels with no additional binning. 488 nm and 561
243  nm lasers were used for excitation. Data was processed using Volocity software (Perkin Elmer) and Adobe Illustrator CS
244  (Adobe). TIRF Imaging was used in all assays, including of fixed cells in Fig. 4. The penetration depth used was set at 150
245  nm to optimise the ratio signal / noise. For motor-dependent endosomal sorting assays, thousand frames were
246  acquired. Colocalization studies were also performed on live cells to keep the tubular structures intact. Image
247  brightness and contrast was adjusted in ImageJ/Fiji and the same processing was applied to all image sets within each
248  experiment.

249  PROCESSING AND QUANTIFICATION OF IMAGE DATA AND STATISTICAL ANALYSIS

250  Maximum intensity projections in Figure 1A, D, G, J, and M were done using Fiji. Colour coding of time sequences was
251  achieved using an ImageJ plug-in developed by Kota Miura (EMBL Heidelberg) which is available at:
252  http://cmci.embl.de/downloads/timeseriescolorcoder and within the Fiji implementation of ImageJ (Schindelin et al.,
253  2012). For these data, the first image of each sequence was extracted from the sequence and then subtracted from the
254  remaining data set to reduce background prior to running the "time series color coder" plugin.

255  Track lengths were measured automatically in Volocity (version 5.4.2, Perkin Elmer) after thresholding to detect only
256  lines >1 μm. Data in Fig. 2 come from measuring >750 objects from 3 independent experiments.

257  Representative images are shown, all experiments were repeated independently at least three times each. Samples
258  were compared using ANOVA with Dunnett's post-hoc test. All images were prepared with Adobe Photoshop CS and
259  Adobe Illustrator CS3.

260  ACKNOWLEDGEMENTS

## CONTRIBUTIONS

## FUNDING

## FIGURE LEGENDS

Figure 1: Projections of time lapse sequence from TIRF imaging of tsO45-G-GFP translocation. Image sequences are comprised of 1000 frames acquired at 12.04 frames per second. (A, D, G, J, M) Maximum intensity projections generated from all 1000 frames. (B, E, H, K, N) enlarged in (C, F, I, L, O) show colour coded time projections of every fourth frame from these sequences (332 ms intervals, 250 frames total). (P) Shows the colour coding for time projections. Scale bars (all frames) = 10 μm.

Figure 2: (A) Proportion of moving objects as a percentage of the total puncta detected. Statistical significance was tested using an ANOVA with a Dunnett's post-hoc test. (B) Quantification of time-lapse imaging. Images were processed to generate maximum intensity projections as shown in Figure 1. Track lengths were then automatically measured in Volocity and plotted. Each spot represents an individual particle. Measurements are derived from 3 independent experiments, 3-8 cells in each experiment, total of 75 objects. Statistical significance was tested using an ANOVA with a Dunnett's post-hoc test. Red asterisks indicate statistically detectable decrease in track length; green asterisks represent a statistically detectable increase in track length.

Figure 3: Increased tubulation of ER-to-Golgi carriers following suppression of DHC1 expression. Examples are taken from the time lapse movie sequence associated with Figure 1D. Boxed regions show 3x enlargements. Time from the start of the image sequence is shown (mins:secs) Bars = 10 μm.

Figure 4: Motor subunit depleted cells expressing tsO45-G-GFP were fixed and immunolabelled to detect COPI (β'-COP). (A) An example of a control (GL2 siRNA transfected) cell. Bar = 10 μm. (B, C) Image quantification was performed manually to determine (B) the number of tsO45-G-GFP puncta with associated COPI labelling and (C) the polarity of these structures with respect to the Golgi apparatus. "Correctly oriented" structures are those with the COPI-positive domain facing away from the Golgi and the tsO45-G-GFP-positive domain facing towards the Golgi. G indicates the user-defined point of the Golgi apparatus. Asterisks in B and C in dictate those cases for which a statistically detectable difference was found using ANOVA with Dunnett's post-hoc test. (D) RPE1 cells were transfected with siRNA against the various motor proteins for 72 hours. The cells were then lysed and after a protein assay equal amounts of protein analyzed by immunoblotting with an anti-KDEL or an anti-α-tubulin antibody. (E) Immunofluorescence labelling of control or KIF5B depleted cells with antibodies directed against giantin or –KDEL bearing proteins. Bar (all panels) = 10 μm.

# REFERENCES

Ally, S., A.G. Larson, K. Barlan, S.E. Rice, and V.I. Gelfand. 2009. Opposite-polarity motors activate one another to trigger cargo transport in live cells. *The Journal of cell biology*. 187:1071-1082.

Burkhardt, J.K., C.J. Echeverri, T. Nilsson, and R.B. Vallee. 1997. Overexpression of the dynamitin (p50) subunit of the dynactin complex disrupts dynein-dependent maintenance of membrane organelle distribution. *The Journal of cell biology*. 139:469-484.

Chen, C.A., and H. Okayama. 1988. Calcium phosphate-mediated gene transfer: a highly efficient transfection system for stably transforming cells with plasmid DNA. *BioTechniques*. 6:632-638.

Derr, N.D., B.S. Goodman, R. Jungmann, A.E. Leschziner, W.M. Shih, and S.L. Reck-Peterson. 2012. Tug-of-war in motor protein ensembles revealed with a programmable DNA origami scaffold. *Science*. 338:662-665.

Franker, M.A., and C.C. Hoogenraad. 2013. Microtubule-based transport - basic mechanisms, traffic rules and role in neurological pathogenesis. *J. Cell Sci.* 126:2319-2329.

Gupta, V., K.J. Palmer, P. Spence, A. Hudson, and D.J. Stephens. 2008. Kinesin-1 (uKHC/KIF5B) is required for bidirectional motility of ER exit sites and efficient ER-to-Golgi transport. *Traffic*. 9:1850-1866.

Ho, W.C., V.J. Allan, G. van Meer, E.G. Berger, and T.E. Kreis. 1989. Reclustering of scattered Golgi elements occurs along microtubules. *Eur. J. Cell Biol.* 48:250-263.

Hunt, S.D., A.K. Townley, C.M. Danson, P.J. Cullen, and D.J. Stephens. 2013. Microtubule motors mediate endosomal sorting by maintaining functional domain organization. *J. Cell Sci.* 126:2493-2501.

Lewis, M.J., and H.R. Pelham. 1990. A human homologue of the yeast HDEL receptor. *Nature*. 348:162-163.

Lippincott-Schwartz, J., N.B. Cole, A. Marotta, P.A. Conrad, and G.S. Bloom. 1995. Kinesin is the motor for microtubule-mediated Golgi-to-ER membrane traffic. *J. Cell Biol.* 128:293-306.

Lippincott-Schwartz, J., J.G. Donaldson, A. Schweizer, E.G. Berger, H.P. Hauri, L.C. Yuan, and R.D. Klausner. 1990. Microtubule-dependent retrograde transport of proteins into the ER in the presence of brefeldin A suggests an ER recycling pathway. *Cell*. 60:821-836.

Lippincott-Schwartz, J., L.C. Yuan, J.S. Bonifacino, and R.D. Klausner. 1989. Rapid redistribution of Golgi proteins into the ER in cells treated with brefeldin A: evidence for membrane cycling from Golgi to ER. *Cell*. 56:801-813.

Mayor, S., J.F. Presley, and F.R. Maxfield. 1993. Sorting of membrane components from endosomes and subsequent recycling to the cell surface occurs by a bulk flow process. *J. Cell Biol.* 121:1257-1269.

Munro, S., and H.R. Pelham. 1987. A C-terminal signal prevents secretion of luminal ER proteins. *Cell*. 48:899-907.

Palmer, K.J., H. Hughes, and D.J. Stephens. 2009. Specificity of cytoplasmic dynein subunits in discrete membrane-trafficking steps. *Mol. Biol. Cell*. 20:2885-2899.

Polishchuk, E.V., A. Di Pentima, A. Luini, and R.S. Polishchuk. 2003. Mechanism of Constitutive Export from the Golgi: Bulk Flow via the Formation, Protrusion, and En Bloc Cleavage of large trans-Golgi Network Tubular Domains. *Mol. Biol. Cell*. 14:4470-4485.

Presley, J.F., N.B. Cole, T.A. Schroer, K. Hirschberg, K.J. Zaal, and J. Lippincott-Schwartz. 1997. ER-to-Golgi transport visualized in living cells. *Nature*. 389:81-85.

Roux, A., G. Cappello, J. Cartaud, J. Prost, B. Goud, and P. Bassereau. 2002. A minimal system allowing tubulation with molecular motors pulling on giant liposomes. *Proc. Natl. Acad. Sci. USA*. 99:5394-5399.

Schindelin, J., I. Arganda-Carreras, E. Frise, V. Kaynig, M. Longair, T. Pietzsch, S. Preibisch, C. Rueden, S. Saalfeld, B. Schmid, J.Y. Tinevez, D.J. White, V. Hartenstein, K. Eliceiri, P. Tomancak, and A. Cardona. 2012. Fiji: an open-source platform for biological-image analysis. *Nature Methods*. 9:676-682.

Shima, D.T., S.J. Scales, T.E. Kreis, and R. Pepperkok. 1999. Segregation of COPI-rich and anterograde-cargo-rich domains in endoplasmic-reticulum-to-Golgi transport complexes. *Curr. Biol.* 9:821-824.

Simpson, J.C., T. Nilsson, and R. Pepperkok. 2006. Biogenesis of tubular ER-to-Golgi transport intermediates. *Mol. Biol. Cell*. 17:723-737.

Stauber, T., J.C. Simpson, R. Pepperkok, and I. Vernos. 2006. A role for kinesin-2 in COPI-dependent recycling between the ER and the Golgi complex. *Current biology : CB*. 16:2245-2251.

Stephens, D.J. 2012. Functional coupling of microtubules to membranes - implications for membrane structure and dynamics. *J. Cell Sci.* 125:2795-2804.

Thyberg, J., and S. Moskalewski. 1985. Microtubules and the organization of the Golgi complex. *Exp. Cell Res.* 159:1-16.

Tomas, M., E. Martinez-Alonso, J. Ballesta, and J.A. Martinez-Menarguez. 2010. Regulation of ER-Golgi intermediate compartment tubulation and mobility by COPI coats, motor proteins and microtubules. *Traffic*. 11:616-625.

Watson, P., R. Forster, K.J. Palmer, R. Pepperkok, and D.J. Stephens. 2005. Coupling of ER exit to microtubules through direct interaction of COPII with dynactin. *Nat. Cell Biol.* 7:48-55.

Yadav, S., M.A. Puthenveedu, and A.D. Linstedt. 2012. Golgin160 recruits the Dynein motor to position the Golgi apparatus. *Dev. Cell*. 23:153-165.

358 SUPPLEMENTARY MATERIAL: MOVIES

359 All movies show TIRF imaging of tsO45-G-GFP 12 minutes after temperature shift of cells to 32$^o$C. Cells were previously
360 transfected with siRNA duplexes as indicated.

361 Movie 1A: GL2-transfected cells. Playback at real time. See Figure 1A.

362 Movie 1B: GL2-transfected cells. Playback at 3x real time. See Figure 1A.

363 Movie 2A: DHC1-transfected cells. Playback at real time. See Figure 1D.

364 Movie 2B: DHC1-transfected cells. Playback at 3x real time. See Figure 1D.

365 Movie 3A: KIF5B-transfected cells. Playback at real time. See Figure 1G.

366 Movie 3B: KIF5B-transfected cells. Playback at 3x real time. See Figure 1G.

367 Movie 4A: KAP3-transfected cells. Playback at real time. See Figure 1J.

368 Movie 4B: KAP3-transfected cells. Playback at 3x real time. See Figure 1J.

369 Movie 5A: LIC1-transfected cells. Playback at real time. See Figure 1M.

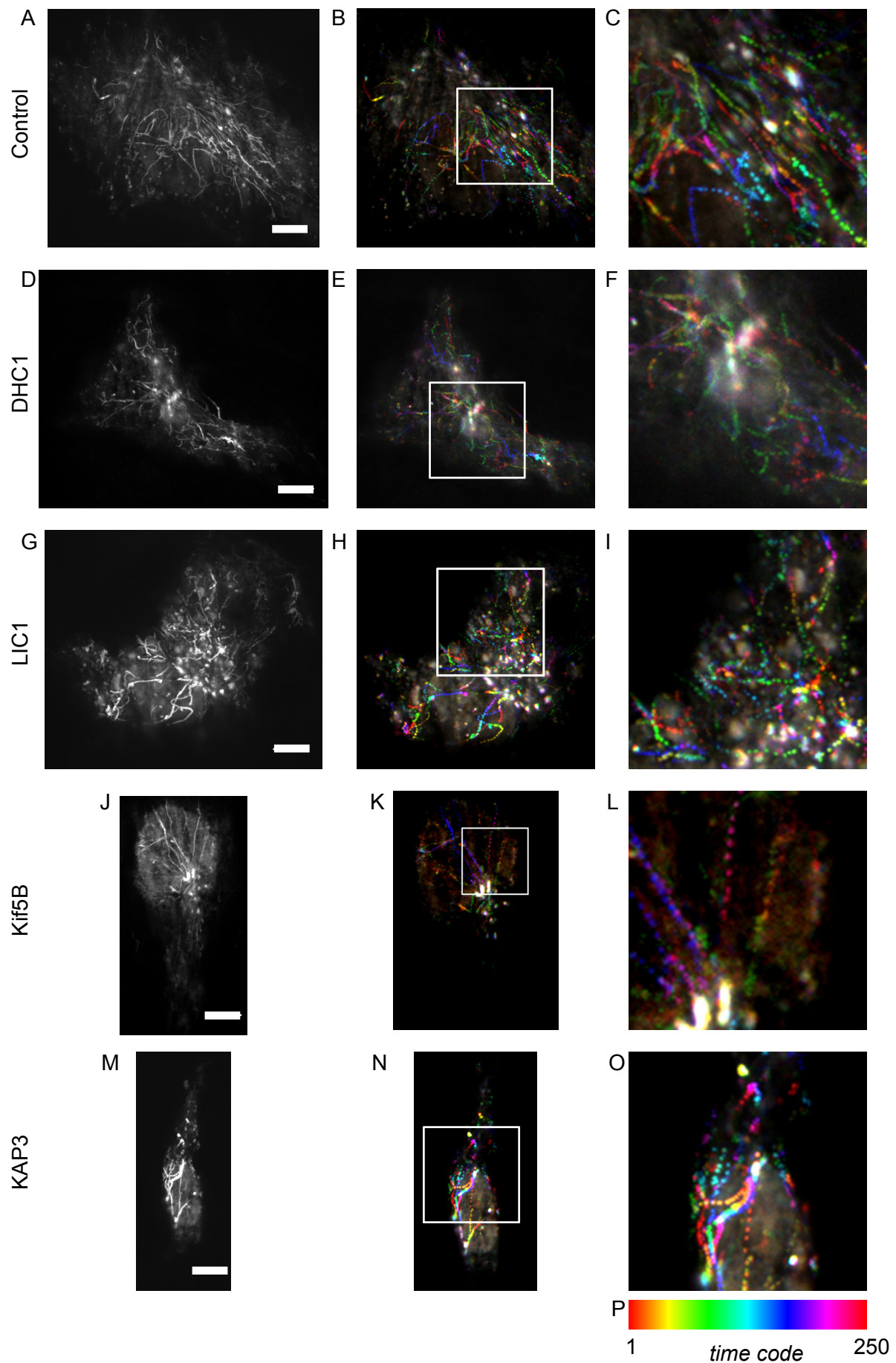370 Movie 5B: LIC1-transfected cells. Playback at 3x real time. See Figure 1M.

Figure 1: Projections of time lapse sequence from TIRF imaging of tsO45-G-GFP translocation. Image sequences are comprised of 1000 frames acquired at 12.04 frames per second. (A, D, G, J, M) Maximum intensity projections generated from all 1000 frames. (B, E, H, K, N) enlarged in (C, F, I, L, O) show colour coded time projections of every fourth frame from these sequences (332 ms intervals, 250 frames total). (P) Shows the colour coding for time projections. Scale bars (all frames) = 10 μm.
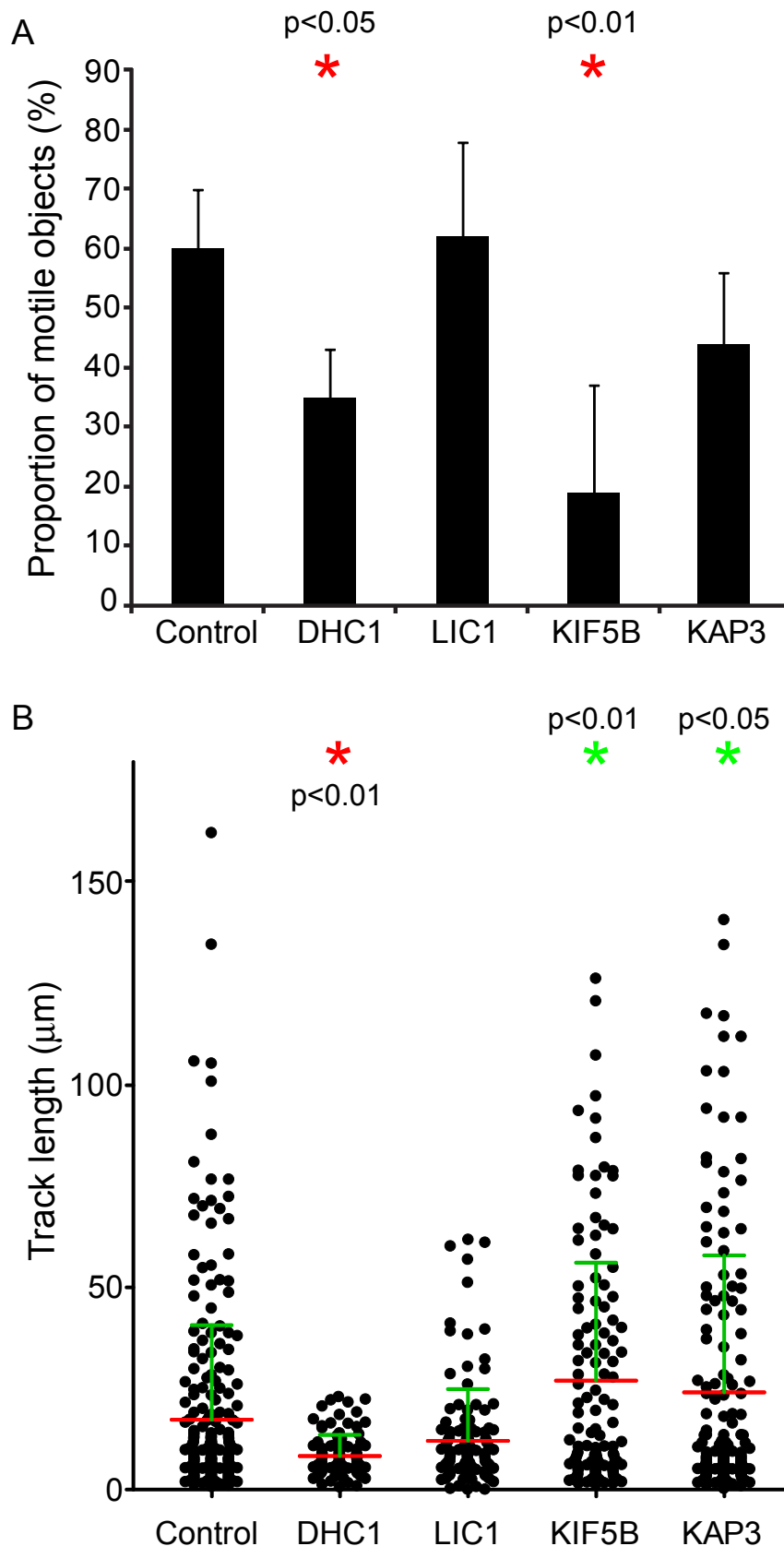
Figure 2: (A) Proportion of moving objects as a percentage of the total puncta detected. Statistical significance was tested using an ANOVA with a Dunnett's post-hoc test. (B) Quantification of time-lapse imaging. Images were processed to generate maximum intensity projections as shown in Figure 1. Track lengths were then automatically measured in Volocity and plotted. Each spot represents an individual particle. Measurements are derived from 3 independent experiments, 3-8 cells in each experiment, total of 75 objects. Statistical significance was tested using an ANOVA with a Dunnett's post-hoc test. Red asterisks indicate statistically detectable decrease in track length; green asterisks represent a statistically detectable increase in track length.
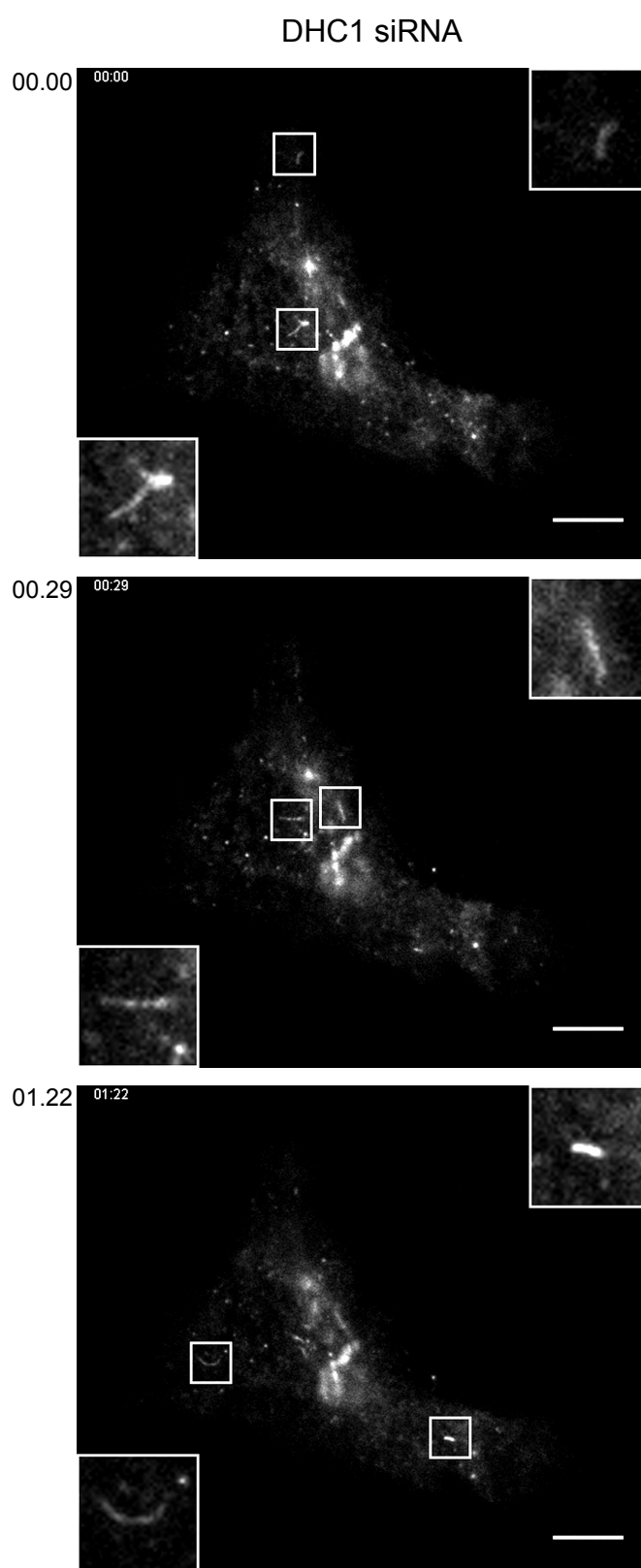
## DHC1 siRNA



Figure 3: Increased tubulation of ER-to-Golgi carriers following suppression of DHC1 expression. Examples are taken from the time lapse movie sequence associated with Figure 1D. Boxed regions show 3x enlargements. Time from the start of the image sequence is shown (mins:secs) Bars = 10 μm.
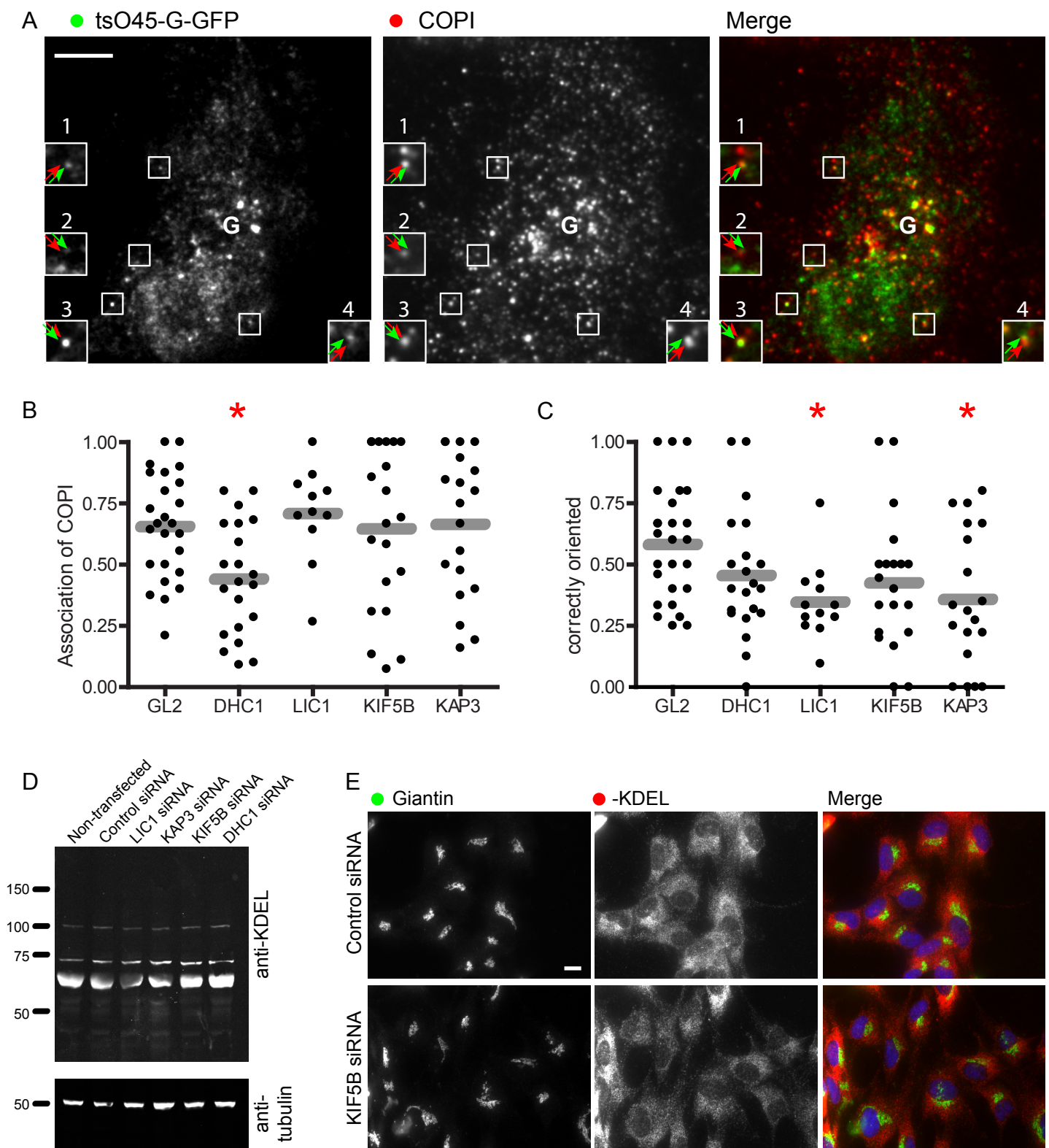
Figure 4: Motor subunit depleted cells expressing tsO45-G-GFP were fixed and immuolaballed to detect COPI (β'-COP). (A) An example of a control (GL2 siRNA transfected) cell. Bar = 10 μm. (B, C) Image quantification was performed manually to determine (B) the number of tsO45-G-GFP puncta with associated COPI labelling and (C) the polarity of these structures with respect to the Golgi apparatus. "Correctly oriented" structures are those with the COPI-positive domain facing away from the Golgi and the tsO45-G-GFP-positive domain facing towards the Golgi. G indicates the user-defined point of the Golgi apparatus. Asterisks in B and C in dictate those cases for which a statistically detectable difference was found using ANOVA with Dunnett's post-hoc test. (D) RPE1 cells were transfected with siRNA against the various motor proteins for 72 hours. The cells were then lysed and after a protein assay equal amounts of protein analyzed by immunoblotting with an anti-KDEL or an anti-α-tubulin antibody. (E) Immunofluorescence labelling of control or KIF5B depleted cells with antibodies directed against giantin or –KDEL. Bar (all panels) = 10 μm.